

MICROSTRUCTURE AND TRANSPORT PROPERTIES OF LITHIUM HEXAFLUOROPHOSPHATE SOLUTIONS IN BINARY MIXTURE OF DIMETHYL CARBONATE WITH ETHYLENE CARBONATE FROM MOLECULAR DYNAMICS SIMULATION

D.S. Dudariev^{*a}, Y.A. Holubenko^{*b}, R.M.N. Jallah^{‡c}, O.N. Kalugin^{*d}


^{*}V. N. Karazin Kharkiv National University, School of Chemistry, 4 Svobody sqr., Kharkiv, 61022 Ukraine

[‡]University of Tripoli, Faculty of Education Janzour, Tripoli, Libya


a) ✉ dima@dudariev@gmail.com

 <https://orcid.org/0000-0002-2556-8036>


b) ✉ sebsalieri@gmail.com

 <https://orcid.org/0009-0005-7075-9017>

c) ✉ r.jallah@uot.edu.ly

 <https://orcid.org/0009-0008-4937-283X>

d) ✉ onkalugin@gmail.com

 <https://orcid.org/0000-0003-3273-9259>

Solutions of Li⁺ salts in many non-aqueous solvents used in Li-ion batteries have a maximum conductivity curve depending on the electrolyte concentration. For the microscopic interpretation of this phenomenon for one of the most popular electrolytes, LiPF₆ solutions in a binary mixture of dimethyl carbonate (DMC) / ethylene carbonate (EC) (1:1), molecular dynamics simulations of the corresponding systems with a salt content of 0.1, 0.5, 1.0, 1.5 and 2.0 M were performed. The potential models for DMC and EC molecules were developed as the combination of two different force fields: OPLS-AA and GAFF in order to properly reproduce the diffusion coefficients of pure solvents. The structure has been analyzed in terms of radial distribution functions (RDFs) and running co-ordination numbers (RCNs). The results show that Li⁺ cation can form contact ion pairs (CIPs) and solvent shared ion pairs (SSIPs) in the solutions. The total coordination number of the cation remains the same at around 5.5-6.0 for all concentrations. Also, EC molecules and PF₆⁻ anions are competing for the position in the first coordination shell of the cation. The aggregate analysis with two different distance criteria was performed: minima on the RDFs and the minima on the second derivative of the RCNs. The diffusion coefficients for all components of the solutions and viscosity of simulated systems were also obtained. The diffusion coefficients for all components are decreasing and viscosity values are non-linearly increasing with the salt concentration increase. The conductivity values were obtained with the diffusion coefficient values of ions via Nernst-Einstein relation. These findings and the drastic viscosity increase at 1.0 M and at higher concentrations of LiPF₆ are in agreement with the calculated experimental conductivity values.

Keywords: lithium hexafluorophosphate, dimethyl carbonate, ethylene carbonate, local structure, transport properties, ionic aggregation.

Introduction

Lithium-ion batteries are widely used in various portable devices [1-5]. They were leading the technological revolution in the electrochemistry for the last decades. The combination of electrode materials, electrolyte solvents and, of course, salts can hugely impact the battery performance [5-17]. Practical electrolyte should be electrochemically stable, have high ionic conductivity, transference number, good electrochemical and thermal stability, low volatility, flammability, toxicity and be cheap in the production [18].

Polar organic molecules such as dimethyl carbonate (DMC) and ethylene carbonate (EC) are one of the most common solvents in lithium batteries [6, 19-21]. Binary mixtures of solvents proved to be useful in improving electrolyte behavior for different temperatures and in optimizing electrochemical and physical properties [22-23]. Electrolytes with EC known to form a stable solid electrolyte interface on anodes that can prevent electrolyte decomposition [24]. EC also has high dielectric constant and relative viscosity. That is why the linear ester DMC with low viscosity and dielectric constant usually is combined with the cyclic ester like EC. The overall viscosity of such mixture is lower than of pure EC, the mixture can still dissolve lithium salts because of high dielectric constant of EC and, most importantly, the ionic conductivity of such system improves [25]. As for the salt, LiPF₆ has a large dissociation degree in organic carbonate solvents, which results in an excellent ionic conductivity for the electrolyte.

© Dudariev D. S., Holubenko Y. A., Jallah R. M. N., Kalugin O. N., 2024



This is an open access article distributed under the terms of the Creative Commons Attribution License 4.0.

Due to these reasons organic polar electrolytes was studied by variety techniques with the accent on electrochemical application. These studies include such methods as vibrational spectroscopy, X-ray diffraction [26], photoelectron spectroscopy [27-28], neutron scattering [29], NMR [30], etc. Although as was mentioned the combination of LiPF_6 with carbonate solvents leads to better electroconductivities of such systems, one needs to choose the composition of the components attentively because the conductivity dependence has maximum on the concentration curve [31-33]. One of the most common commercial used solutions of LiPF_6 in DMC/EC (1:1) binary has the peak electrical conductance at 1 M [33-34]. This maximum usually explained via local structure changes in the solution [35], although the literature data are of a qualitative nature without a detailed analysis of the contribution of ion aggregation to the formation of a maximum on the concentration curve of electrical conductivity.

In this paper, molecular dynamics (MD) simulations were performed to obtain microstructural and transport properties for LiPF_6 in DMC/EC (1:1) binary mixture with the salt concentration of 0.1, 0.5, 1.0, 1.5 and 2.0 M. In addition, the aggregate analysis has been performed to study the features of ionic clusterization in lithium salt solutions.

Methodology

Details of molecular dynamics simulation. MD simulations of the LiPF_6 and binary mixtures of DMC/EC (1:1) have been performed at five different compositions. To calculate the exact number of the ions and solvent molecules for the MD simulation from the molarities the experimental densities, ρ , of the LiPF_6 in DMC/EC (1:1) binary mixture were used [36-37]. The number of the different particles in cubic box and molar concentration of the LiPF_6 in the simulated systems are collected in Table 1. The total number of Li^+ cations and PF_6^- anions were always equal to 100.

Two systems of pure solvents (DMC and EC) were also simulated (with the number of molecules of 500 for each). Pure EC system was simulated at the temperature of 313.15 K because at 298.15 K this solvent is solid substance.

All simulations have been carried out using the GROMACS 2019.4 software package [38]. The temperature of 298.15 K and pressure (in *NPT* ensemble) of 1 bar were kept constant by velocity-rescaling thermostat [39] and the Berendsen barostat [40]. The relaxation times were, 0.1 ps and 0.5 ps, respectively. The equations of motion were integrated via leap-frog algorithm, time step of all simulations was equal to 0.5 fs. The long-range part of the electrostatic interaction has been accounted for by the Particle Mesh Ewald method [41] with the cutoff radius of 1.0 nm. Lennard-Jones interactions were treated with the conventional shifted force technique. The Lennard-Jones parameters corresponding to unlike pairs of atoms have been calculated by the standard Lorentz-Berthelot combination rules [42]. After equilibrating the systems (*NPT* ensemble), simulations of 10 ns have been performed (*NVT* ensemble). All systems were simulated five times from new independent randomly created configuration. The last 1 ns of the trajectory of the simulations have then been used for the structural analysis while full 10 ns trajectories were used for transport properties calculation.

Table 1. The composition of the simulated systems of LiPF_6 in DMC/EC (1:1) binary mixture.

LiPF_6 concentration	Number of Li^+	Number of PF_6^-	Number of DMC	Number of EC	ρ [36-37], g/ cm^3
0.1 M	100	100	6707	6707	1.21
0.5 M	100	100	1318	1318	1.25
1.0 M	100	100	664	664	1.29
1.5 M	100	100	420	420	1.33
2.0 M	100	100	308	308	1.36

Force field refinement. The structure of the PF_6^- anion and DMC and EC solvent molecules along with the atomic labeling scheme is shown at Figure 1.

For the Li^+ the potential model directly from OPLS-AA [43] has been used.

For the PF_6^- anion the potential model from Canongia Lopes et al. [44] was taken.

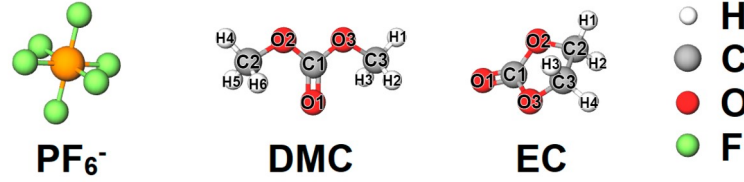


Figure 1. Structure of the PF_6^- anion and molecular solvents of DMC and EC. The labeling of solvent molecules used in potential models is also shown.

As a first step the LigParGen [45] was used to develop Lennard-Jones (LJ) parameters, as well as bond, angle, and dihedral angle parameters based on the OPLS-AA [43, 46-47] force field for both DMC and EC.

In current study the total potential energy was reproduced by the sum of intra- and intramolecular contributions:

$$\begin{aligned}
 U_{tot} = & \sum_{ij}^{\text{bonds}} \frac{k_{r,ij}}{2} (r_{ij} - r_{0,ij})^2 + \sum_{ijk}^{\text{angles}} \frac{k_{\theta,ijk}}{2} (\theta_{ijk} - \theta_{0,ijk})^2 + \sum_{ijkl}^{\text{dihedral}} \sum_{n=0}^5 C_n (\cos(\psi_{ijkl}))^n + \\
 & + \sum_{ijkl}^{\text{improper}} k_{\phi,ijkl} (1 + \cos(n\phi_{ijkl} - \phi_{s,ijkl})) + \sum_{ij}^{\text{nonbonded}} \left(4\varepsilon_{ij} \left[\left(\frac{\sigma_{ij}}{r_{ij}} \right)^{12} - \left(\frac{\sigma_{ij}}{r_{ij}} \right)^6 \right] + \frac{q_i q_j}{4\pi\varepsilon_0 r_{ij}} \right), \quad (1)
 \end{aligned}$$

where k is the force constant for bond stretching (r), angle bending (θ), proper and improper dihedral (ϕ), respectively, ε and σ are the Lennard-Jones energy and the distance parameters, respectively, and q stands for the fractional charges of the interaction sites. For proper dihedral $\psi_{ijkl} = 180^\circ - \phi_{ijkl}$. All the intramolecular parameters for DMC and EC force field models are listed in the Table 2.

Optimization of the starting geometry and calculation of partial charges of atoms was carried out using the software package Gaussian16 [48] at M062X/AUG-cc-PVTZ level. The algorithm for calculating partial atomic charges according to Breneman was applied [49-50]. The charges obtained are presented in the Table 2.

The results obtained for diffusion coefficients (D) of pure solvents are much lower than the experimental ones. For pure DMC and EC diffusion coefficient was equal to $1.5 \cdot 10^{-5} \text{ cm}^2/\text{s}$ and $0.5 \cdot 10^{-5} \text{ cm}^2/\text{s}$, respectively, as compare with experimental values of $2.6 \cdot 10^{-5} \text{ cm}^2/\text{s}$ (at 303 K) and $0.8 \cdot 10^{-5} \text{ cm}^2/\text{s}$, respectively [51].

In order to improve the results for the solvent potential models and to reproduce transport properties of pure molecular liquids the original OPLS-AA models were modified. Following our guess, lowering the effective molecule radius can improve the diffusion coefficients. Thus, the Lennard-Jones parameters of H atoms of DMC and EC were replaced with the GAFF force field ones [52-53]. The GAFF ε parameter is almost two times lower than such of OPLS-AA force field. The Lennard-Jones parameters and charges of the DMC and EC are shown in the Table 2.

The obtained results for density, self-diffusion coefficient and enthalpy of vaporization for the pure solvents in the comparison with the experimental data are shown in the Table 3. For the potential models with the H parameters from GAFF the results are close to the experimental values. For further MD simulations these modified potential models were selected.

Table 2. Charge distribution, q , Lennard-Jones parameters, σ and ε , intramolecular parameters, k_i , for DMC and EC. Asterisk represents the Lennard-Jones parameters of the GAFF for H atoms that replaced the original ones

DMC			EC	
Charge	q, e		q, e	
O ¹	-0.597267		-0.563993	
O ²⁻³	-0.449998		-0.396963	
C ¹	1.004995		0.878357	
C ²⁻³	0.098148		0.167807	
H ¹	0.035715		0.035874	
H ²	0.035720		0.036100	
H ³	0.076551		0.035878	
H ⁴	0.035718		0.036096	
H ⁵	0.035717			
H ⁶	0.076551			
Atom	σ, nm	$\varepsilon, \text{kJ/mol}$	σ, nm	$\varepsilon, \text{kJ/mol}$
O ¹	0.296	0.87864	0.296	0.87864
O ²⁻³	0.290	0.58576	0.290	0.58576
C ¹	0.355	0.29288	0.355	0.29288
C ²⁻³	0.350	0.276144	0.350	0.276144
H ¹⁻⁴			0.250 (0.2471)*	0.12552 (0.065693)*
H ¹⁻⁶	0.250 (0.2471)*	0.12552 (0.065693)*		
Bond	r_0, nm	$k_r, \text{kJ}/(\text{mol}\cdot\text{nm}^2)$	r_0, nm	$k_r, \text{kJ}/(\text{mol}\cdot\text{nm}^2)$
C ¹ -O ¹	0.1229	476976.0	0.1229	476976
C ¹ -O ¹⁻²	0.1327	179075.2	0.1327	179075.2
C ² -C ³			0.1529	224262.4
C ² -O ²	0.141	267776.0	0.141	267776.0
C ³ -O ³	0.141	267776.0	0.141	267776.0
C ² -H ¹⁻²			0.109	284512.0
C ² -H ¹⁻³	0.109	284512.0		
C ³ -H ³⁻⁴			0.109	284512.0
C ³ -H ⁴⁻⁶	0.109	284512.0		
Angle	θ_0, deg	$k_\theta, \text{kJ}/(\text{mol}\cdot\text{rad}^2)$	θ_0, deg	$k_\theta, \text{kJ}/(\text{mol}\cdot\text{rad}^2)$
O ¹ -C ¹ -O ¹⁻²	123.4	694.544	123.4	694.544
C ¹ -O ² -C ²	116.9	694.544	116.9	694.544
C ¹ -O ³ -C ³	116.9	694.544	116.9	694.544
C ² -C ³ -O ³			109.5	418.4
C ³ -C ² -O ³			109.5	418.4
C ² -C ³ -H ³⁻⁴			110.7	313.8
C ³ -C ² -H ¹⁻²			110.7	313.8
O ² -C ¹ -O ³	118.18	584.923	118.18	584.923
O ² -C ² -H ¹⁻²			109.5	292.88
O ² -C ² -H ¹⁻³	109.5	292.88		
O ³ -C ³ -H ³⁻⁴			109.5	292.88
O ³ -C ³ -H ⁴⁻⁶	109.5	292.88		
H ¹ -C ² -H ²	107.8	276.144	107.8	276.144
H ³ -C ² -H ¹⁻²	107.8	276.144		
H ³ -C ³ -H ⁴			107.8	276.144
H ⁴ -C ³ -H ⁵	107.8	276.144		
H ⁶ -C ³ -H ⁴⁻⁵	107.8	276.144		

Table 2 continued

Improper	ϕ_s , deg	k_ϕ , kJ/mol	n	ϕ_s , deg	k_ϕ , kJ/mol	n
O ¹ -O ² -C ¹ -O ³	180.0	43.932	2			
O ³ -C ¹ -O ¹ -O ²				180.0	43.932	2
Dihedral	C_0 , kJ/mol	C_1 , kJ/mol	C_2 , kJ/mol	C_3 , kJ/mol	C_4 , kJ/mol	C_5 , kJ/mol
DMC						
C ¹ -O ² -C ² -H ¹⁻³	0.414	1.243	0.0	-1.657	0.0	0.0
C ¹ -O ³ -C ³ -H ⁴⁻⁶	0.414	1.243	0.0	-1.657	0.0	0.0
O ¹ -C ¹ -O ² -C ²	21.439	0.0	-21.439	0.0	0.0	0.0
O ¹ -C ¹ -O ³ -C ³	21.439	0.0	-21.439	0.0	0.0	0.0
C ² -O ² -C ¹ -O ³	31.206	-9.768	-21.439	0.0	0.0	0.0
C ³ -O ³ -C ¹ -O ²	31.206	-9.768	-21.439	0.0	0.0	0.0
EC						
C ¹ -O ² -C ² -O ³	-2.197	5.201	0.527	-3.531	0.0	0.0
C ¹ -O ³ -C ³ -O ²	-2.197	5.201	0.527	-3.531	0.0	0.0
C ¹ -O ² -C ² -H ¹⁻²	0.414	1.243	0.0	-1.657	0.0	0.0
C ¹ -O ³ -C ³ -H ³⁻⁴	0.414	1.243	0.0	-1.657	0.0	0.0
O ¹ -C ¹ -O ² -C ²	21.439	0.0	-21.439	0.0	0.0	0.0
O ¹ -C ¹ -O ³ -C ³	21.439	0.0	-21.439	0.0	0.0	0.0
C ² -O ² -C ¹ -O ³	31.206	-9.768	-21.439	0.0	0.0	0.0
C ³ -O ³ -C ¹ -O ²	31.206	-9.768	-21.439	0.0	0.0	0.0
O ² -C ² -C ³ -O ³	-1.151	1.151	0.0	0.0	0.0	0.0
O ² -C ² -C ³ -H ³⁻⁴	0.979	2.937	0.0	-3.916	0.0	0.0
O ³ -C ³ -C ² -H ¹⁻²	0.979	2.937	0.0	-3.916	0.0	0.0
H ¹⁻² -C ² -C ³ -H ³⁻⁴	0.628	1.883	0.0	-2.51	0.0	0.0

Table 3. Observed density, ρ , self-diffusion coefficient, D , and enthalpy of vaporization, ΔH_{vap} , and share viscosity, η , calculated at 298.15 K for DMC and at 313.15 K for EC in comparison with the results obtained through experimental measurements.

Property	DMC (298.15 K)		EC (313.15 K)	
	MD	Exp.	MD	Exp.
ρ , g/dm ³	1038	1057 [54]	1294	1321 [54]
$D \cdot 10^5$, cm ² /s	2.2	2.6 ^a [51]	0.6	0.8 [51]
$\Delta_{vap}H$, kJ/mol	35.5	38.0 [55]	54.8	60 [56]

a – for 303 K.

Results and discussion

Microstructural properties. The microstructural properties of LiPF₆ in DMC/EC (1:1) binary mixture were analyzed in terms of radial distribution functions (RDF) and running coordination numbers (RCN). For all RDFs the center atom P of anion as well as most electronegative atom of solvent (the carbonyl O atom for DMC and EC) has been chosen for the analysis.

The RDFs and RCNs between Li⁺ and carbonyl O atoms of solvents DMC and EC for all concentrations are presented at Figure 2.

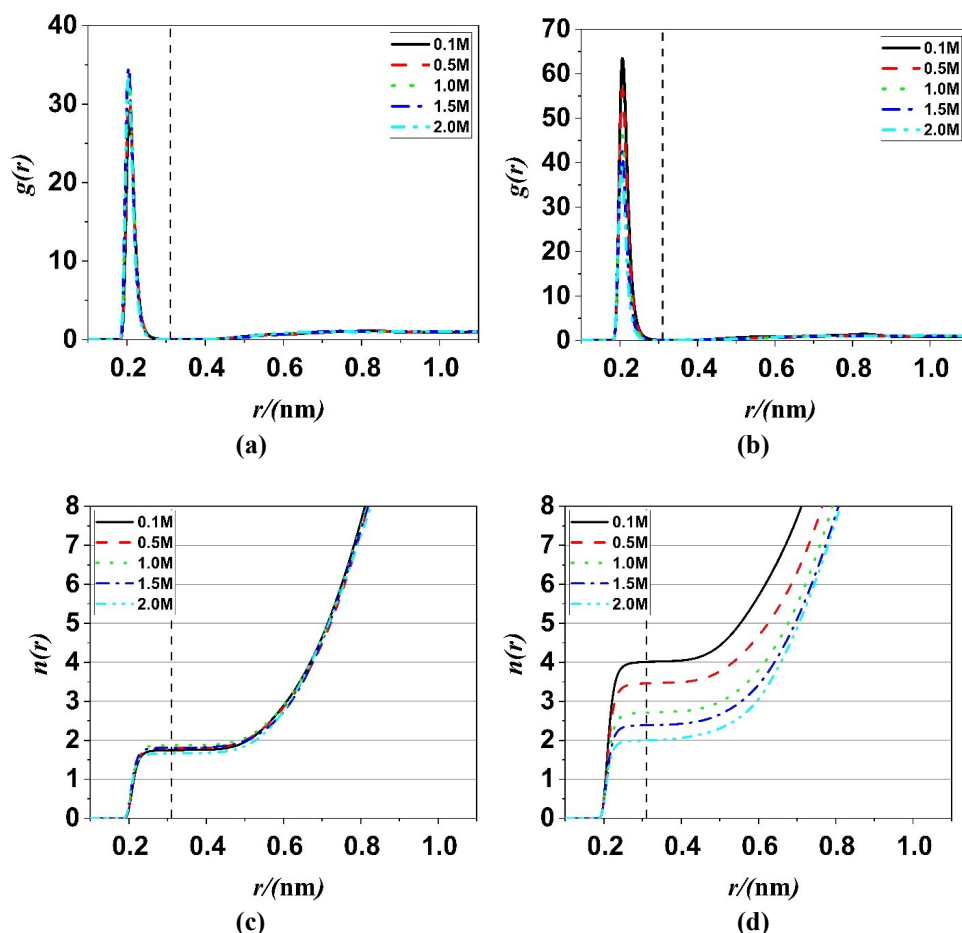


Figure 2. Cation-solvent radial distribution functions (*a* – Li-ODMC; *b* – Li-O_{EC}) and running coordination numbers (*c* – Li-ODMC; *d* – Li-O_{EC}) at various molar concentration of LiPF₆ in DMC/EC (1:1) binary mixture. The vertical dashed line corresponds to the radius of the first solvation shell.

All positions at curves are remained unchanged at different concentrations. Thin sharp first peaks without any shoulders at both cation-solvent RDFs can be observed that indicate the sturdy first solvation shell. The first maxima of RDFs are at approximately 0.20 nm as well as first minima at 0.31 nm for both solvents. This agrees well with time-of-flight neutron diffraction measurements for LiPF₆ in PC with Li-O peak at approximately 0.20 nm [29]. Similar peaks from MD simulations for lithium salts in DMC, EC or PC have value of 0.19-0.20 nm [54, 57-60]. The heights of the Li-ODMC curves almost do not change with the concentration increase of the salt while Li-O_{EC} curves' heights become lower.

The cation-anion RDFs and RCNs for all systems are presented in Figure 3. Here similar curves for all of the concentrations of LiPF₆ in DMC/EC binary mixture can be seen. The first high sharp peak indicates a structured first coordination shell with maximum at approximately 0.34 nm. These peaks as well as the ones in cationic-solvent RDFs (Figure 2a and 2b) are much higher and thinner than relative cation-anion and cation-solvent peaks in the mixtures of ionic liquids with molecular solvents. It corresponds to the classical MD simulation results with a polarizable force field of LiPF₆ in DMC/EC [54]. The small shoulder on all curves with its local maximum near 0.29 nm can be detected. This indicates the occurrence of different mutual cation-anion configuration at these Li-P distance values. The example of cation-anion relative disposition at these distances was obtained from GROMACS trajectory files via VMD program package [61] and shown at Figure 4a. The first maximum of RDFs here (0.34 nm) corresponds to the monodentate linkage of the anion to the cation when Li⁺ is close to only one of the F atoms of anion. Thus, the local maximum of shoulder (0.29 nm) corresponds to the position of anion when Li⁺ is close to two or even three F atoms of anion at the same time (bidentate and tridentate linkage respectively). The first minimum of RFDs is approximately at 0.45 nm.

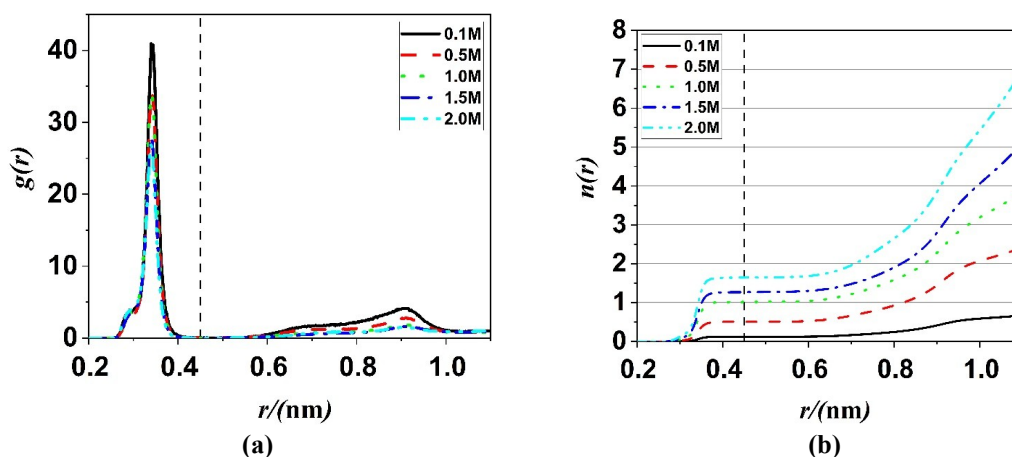


Figure 3. Cation-anion (Li-P) radial distribution functions (a) and running coordination number (b) at various molar concentration of LiPF_6 in DMC/EC (1:1) binary mixture. The vertical dashed line corresponds to the first coordination shell.

As was stated in the literature, contact ion pairs (CIP) and solvent shared ion-pair (SSIP) may occur in the solutions of lithium salts [33, 62-63]. The latter are formed when the solvent molecule (DMC or EC for investigated solutions) is located between cation and anion. After the first minimum all of the RDFs (Figure 3a) have wide plateau until approximately 0.6 nm, and second maximum occurs only at 0.91 nm, second minimum – at 1.04 nm. The wide region, related to the formation of SSIPs, of uncertain position of PF_6^- anion relatively to Li^+ cation (0.6 nm – 1.0 nm on RDFs) can be explained with the packing of solvent molecules around the cation. It was proposed that solvent molecules are arranged around the Li^+ cation in a way that leaves large holes between them. The anions can penetrate into these empty spaces quite closely to the cation [33, 62-63]. Similar phenomenon can be observed in our investigation. The example of such configuration is shown at Figure 4b. The height of each peak at RDF decreases with the increase of the salt concentration.

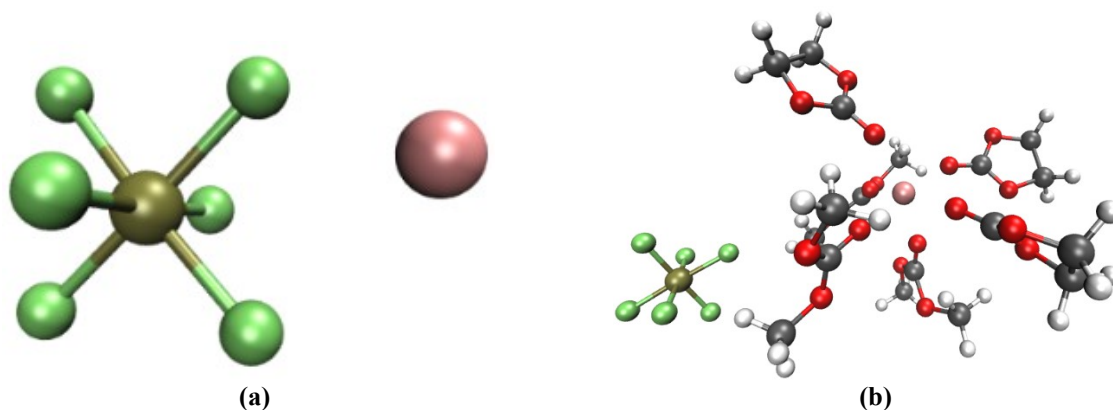


Figure 4. Example of cation-anion contact ion pair (a) and solvent-shared ion pair (b).

It was expected that the coordination numbers for cation-solvent interactions (Figure 2c and 2d) will decrease while the cation-anion ones (Figure 3b) will increase with the increasing of the LiPF_6 concentration. The EC carbonyl O atoms are competing with the PF_6^- anions for the coordination with the Li^+ cation. But in the case of DMC its number is independent of the concentration of the salt. It remains ~ 1.8 for all systems while for Li-P it increases from 0.1 to 1.6 and for EC it decreases from 4 to 2 with the increasing of LiPF_6 concentration in DMC/EC binary mixture. This is caused by higher molecular dipole moment of EC comparing to DMC. Also, EC molecule is smaller and can be packed more efficiently in the Li^+ first coordination sphere than wide and linear DMC. The average total coordination number remains 5.5-6.0 regardless of the concentration. These results are in agreement with previous MD simulations [64].

Ion association. In order to study the association of ions one should to identify the criterion by which two ions can be considered as a part of one aggregate (or cluster). Such a criterion was proposed in different works [65-66] as the distance between coordination centers of respective ions. Thus, two ions were considered to belong to the same associate if their respective centers are located at the equal or lower distance that was chosen as a criterion from each other [67].

Aggregate analysis has been performed by AGGREGATES 3.2.0 software package [68].

To analyze the formation of the aggregates on the solution two distance criteria are proposed. The first is the first minimum in cation-anion RDF (0.45 nm, Figure 3a) which indicates the first coordination sphere around the Li^+ cation. The second criterion was determined by the minimum at the second derivative of cation-anion RCN (0.35 nm, Figure 5). This value shows the distance at which the RCN curves come into plateau regime at which the coordination number have almost no change at all.

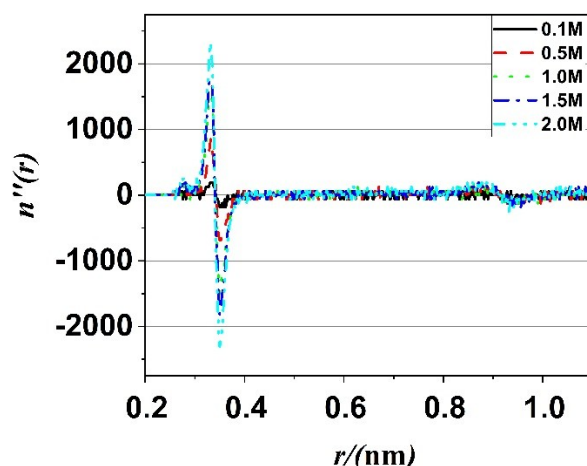


Figure 5. Second derivatives of cation-anion (Li-P) running coordination numbers at various molar concentration of LiPF_6 in DMC/EC (1:1) binary mixture.

The results of the association analysis can be found in Figure 6.

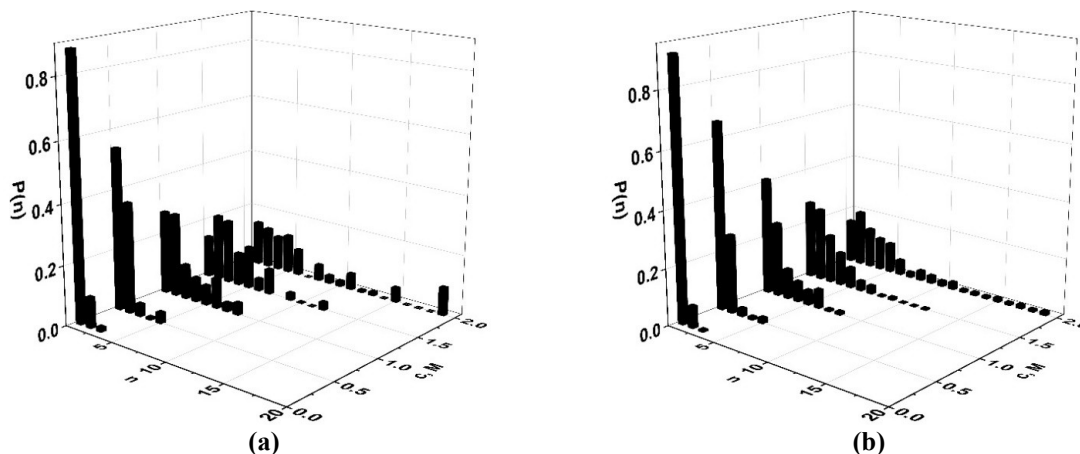


Figure 6. Probability distributions of aggregate sizes with respective first (a) and second (b) criterion at various molar concentration of LiPF_6 in DMC/EC (1:1) binary mixture.

The results are pretty similar for both criteria chosen. The ions are mostly isolated from each other in 0.1 M solution of LiPF_6 in DMC/EC (1:1) binary mixture. With the increasing of the salt concentration, one can see that more and more aggregates of different sizes start to appear. At the same time the number of the free ions decreases. Nevertheless, at the 2.0 M concentration still the size of biggest ionic associate is 19 for both criteria. This fact, ones again, proves the strong solvation effect comparing to the association which is still not dominant even at high concentrations of salt.

To illustrate the general result among all concentrations the average number of associations were obtained (Figure 7). It can be seen that both criteria are similar in their values.

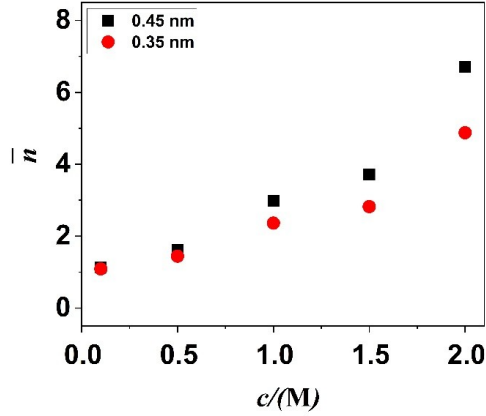


Figure 7. Average numbers of association with both criteria at various molar concentration of LiPF_6 in DMC/EC (1:1) binary mixture.

The ionic conductivity is related to the effective concentration of the charge carriers in the solution according to the Nernst-Einstein relation [69]. The formation of CIPs and SSIPs in the solution and the formation of the ionic clusters as a result reduces the number of charge carriers and thus lowers conductivity. That is why the concentration at which the massive clusterization of ions in aggregate analysis occurs for the second set of criteria is close to the concentration at which the experimental conductivity has maximum at its curve [33].

Transport properties. The transport properties were studied in terms of diffusion coefficients of all the components of the LiPF_6 in DMC/EC binary mixture systems as well as their shear viscosity.

The diffusion constants were obtained by the time integral of velocity autocorrelation function via Green-Kubo integral formula:

$$D = \frac{1}{3} \int_0^{\infty} C_{vv}(t) dt. \quad (2)$$

It should be noted that the values of diffusion coefficients are averaged among the whole system for all the molecules.

For the viscosity a nonequilibrium periodic perturbation method has been used [70]. According to the Navier-Stokes equation:

$$p \frac{\partial u}{\partial t} + p(u \cdot \nabla)u = pa - \nabla p + \eta \nabla^2 u, \quad (3)$$

where u is the velocity of the liquid, a – external force. Suppose the force is applied only in the x direction. In this case the velocity along y and z will be zero:

$$p \frac{\partial u_x(z)}{\partial t} = pa_x(z) + \eta \frac{\partial^2 u_x(z)}{\partial z^2}, \quad (4)$$

The velocity profile as well as acceleration should be periodic because of the periodic system in the simulations. Thus, the cosine function can be used for this purpose:

$$a_x(z) = \Lambda \cos(kz), \quad k = 2\pi/l_z \quad (5,6)$$

where l_z is the height of the box, Λ – acceleration amplitude of the external force. The viscosity then can be obtained:

$$\eta = \frac{\Lambda p}{V k^2}. \quad (7)$$

The measured viscosity greatly depends on the parameter Λ . To obtain the viscosity at zero acceleration few viscosities for different accelerations should be obtained. Then plotting the viscosities versus the amplitudes allows to obtain shear viscosity for $\Lambda=0$ via extrapolation.

The obtained values for diffusion coefficients of all components in the system and the viscosity of the mixtures are presented at Figure 8.

Here it is seen the decreasing of all diffusion coefficients as the concentration of LiPF_6 increases from 0.1 M to 2.0 M. Also, it can be seen that diffusion coefficients of solvent molecules are approximately two times larger than of ions. The values of coefficients for both solvents are similar to each other with less solvated DMC being higher.

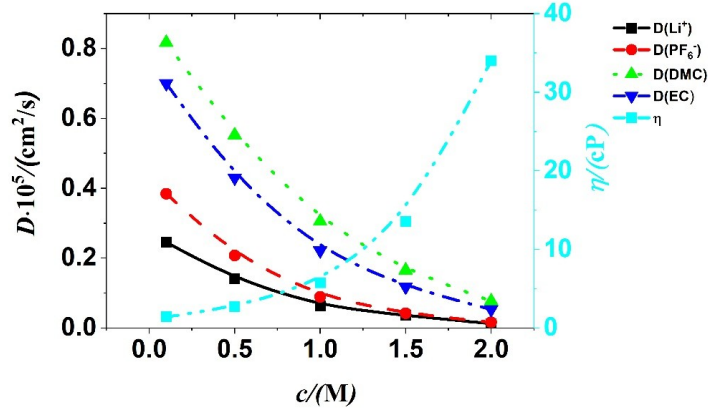


Figure 8. Diffusion coefficients for cation, anions and solvent molecules and viscosity values at various molar concentration of LiPF_6 in DMC/EC (1:1) binary mixture. The error in the calculation of the corresponding values was estimated to be a few percent.

Simultaneously, the viscosity of the system increases according to a non-linear dependence and at highest concentrations investigated it reaches rather huge values of ~ 35 cP. The viscosity behavior can be explained by the increasing in size clusters in the simulated system with the formation of SSIPs in solution beginning after the 1.0 M concentrations of LiPF_6 .

Diffusion coefficients of ions is one of the factors that affects the electric conductivity as stated by Nernst-Einstein relation [69]:

$$\kappa = \frac{e^2}{Vk_B T} (N_+ z_+^2 \bar{D}_+ + N_- z_-^2 \bar{D}_-), \quad (8)$$

where e is the elementary charge, k_B – Boltzmann constant, V – volume of the system, T – temperature of the system, z_{\pm} – charge of the ion, N_{\pm} – number of cations and anions.

The conductivity values obtained from the equation 8 are presented at Figure 9. It is worth mentioning that the highest value of the conductivity appears for the 0.5 M concentration of the LiPF_6 salt, while the experimental value is approximately at 1.0 M [33-34]. This result together is in agreement with the previous observations about ionic association and viscosity increase with the increasing of the salt concentration.

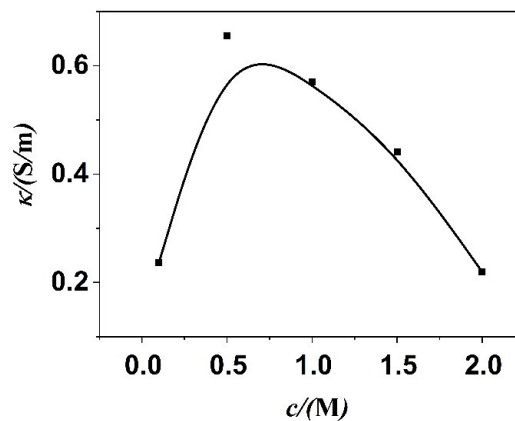


Figure 9. Conductivity values at various molar concentration of LiPF_6 in DMC/EC (1:1) binary mixture.

Conclusions

In the present work LiPF_6 in DMC/EC (1:1) binary mixture solutions of five different concentrations have been studied with classical MD simulation technique. The potential models for

DMC and EC molecules were optimized in this work from the combination of two different force fields: OPLS-AA and GAFF in order to properly reproduce the transport properties of these solvents.

The structure has been analyzed in terms of cation-solvent and cation-anion RDFs and RCNs. The snapshot from the trajectory files of the simulation confirmed the RDF and RCN data and showed that Li^+ cations tend to form contact ion pairs as well as solvent-shared ion pairs.

The RCNs showed that total coordination number of the cation for the first coordination sphere remains 5.5-6.0 for all concentrations. In particular, for DMC it remains ~ 1.8 , while for EC it decreases from 4 to 2 and for PF_6^- anion it increases from 0.1 to 1.6 with the increasing of the salt concentration. This indicates that EC solvent and anions are competing for the position in first coordination sphere.

For the ionic aggregate analysis two criteria were proposed (based on two different distances: minima on the RDFs and the minima on the second derivative of the RCNs). With the increasing of the salt concentration in the simulated systems the larger aggregates start to appear while the number of free ions begin to decrease. The results for distances of minimum on the RDFs or minimum on the second derivative on the RCNs are not differ significantly.

Lastly, the transport properties of simulated systems were obtained. The diffusion coefficients for all components are decreasing and viscosity values are non-linearly increasing with the salt concentration increase. The drastic non-linear increase of the viscosity from nearly 1.0 M and for higher concentrations of LiPF_6 also occurs. The values of the conductivity from the diffusion coefficient values of ions via Nernst-Einstein relation were also obtained. These findings are consistent with the maximum of experimental electroconductivity.

Acknowledgement

The authors acknowledge the Ministry of Education and Science of Ukraine for the Grant No. 0121U112886. The calculations were performed on the *Dell EMC PowerEdge R740 supercomputer* of the Center for collective use of scientific equipment "*Laboratory of micro- and nano-systems, new materials and technologies*" of the Ministry of Education and Science of Ukraine at V.N. Karazin Kharkiv National University. The authors are grateful also to the management of the Université Côte d'Azur, Nice, France, for the opportunity to conduct calculations using the resources of the *Azzurra HPC center*.

References

1. Wang Y., Liu B., Li Q., Cartmell S., Ferrara S., Deng Z. D., Xiao J. Lithium and lithium ion batteries for applications in microelectronic devices: A review. *J. Power Sources* **2015**, 286 330-345. <https://doi.org/10.1016/j.jpowsour.2015.03.164>
2. Liu J., Liu Pacifi J. Addressing the grand challenges in energy storage. *Adv. Funct. Mater.* **2013**, 23 (8), 924-928. <https://doi.org/10.1002/adfm.201203058>
3. Liang Y., Zhao C. Z., Yuan H., Chen Y., Zhang W., Huang J. Q., Yu D., Liu Y., Titirici M. M., Chueh Y. L., et al. A review of rechargeable batteries for portable electronic devices. *InfoMat* **2019**, 1 (1), 6-32. <https://doi.org/10.1002/inf2.12000>
4. Chapter 2 - characteristics of batteries for portable devices. In *Batteries for portable devices*, Pistoia, G., Ed. Elsevier Science B.V.: Amsterdam, **2005**; pp 17-27. <https://doi.org/10.1016/B978-044451672-5/50002-8>
5. Pistoia G. Applications – portable | portable devices: Batteries. In *Encyclopedia of electrochemical power sources*, Garche, J., Ed. Elsevier: Amsterdam, **2009**; pp 29-38. <https://doi.org/10.1016/B978-044452745-5.00358-0>
6. Xu K. Nonaqueous liquid electrolytes for lithium-based rechargeable batteries. *Chem. Rev.* **2004**, 104 (10), 4303-417. <https://doi.org/10.1021/cr030203g>
7. Julien C., Mauger A., Vijn A., Zaghbi K. *Lithium batteries: Science and technology*. Springer Cham: **2016**; p 619. <https://doi.org/10.1007/978-3-319-19108-9>
8. Whittingham M. S. Lithium batteries and cathode materials. *Chem. Rev.* **2004**, 104 (10), 4271-301. <https://doi.org/10.1021/cr020731c>

9. Ye X., Wu J., Liang J., Sun Y., Ren X., Ouyang X., Wu D., Li Y., Zhang L., Hu J., et al. Locally fluorinated electrolyte medium layer for high-performance anode-free li-metal batteries. *ACS Appl. Mater. Interfaces* **2022**, *14* (48), 53788-53797. <https://doi.org/10.1021/acsami.2c15452>
10. Nam K. H., Jeong S., Yu B. C., Choi J. H., Jeon K. J., Park C. M. Li-compound anodes: A classification for high-performance li-ion battery anodes. *ACS Nano* **2022**, *16* (9), 13704-13714. <https://doi.org/10.1021/acsnano.2c05172>
11. Wu F., Yushin G. Conversion cathodes for rechargeable lithium and lithium-ion batteries. *Energ. Environ. Sci.* **2017**, *10* (2), 435-459. <https://doi.org/10.1039/C6EE02326F>
12. Srivastava N., Singh S. K., Meghnani D., Mishra R., Tiwari R. K., Patel A., Tiwari A., Singh R. K. Molybdenum-doped li/mn-rich layered transition metal oxide cathode material $\text{Li}_{1.2}\text{Mn}_{0.6}\text{Ni}_{0.1}\text{Co}_{0.1}\text{O}_2$ with high specific capacity and improved cyclic stability for rechargeable li-batteries. *ACS Appl. Energy Mater.* **2022**, *5* (10), 12183-12195. <https://doi.org/10.1021/acsaem.2c01680>
13. Rodrigues M. T. F., Babu G., Gullapalli H., Kalaga K., Sayed F. N., Kato K., Joyner J., Ajayan P. M. A materials perspective on li-ion batteries at extreme temperatures. *Nat. Energy* **2017**, *2* (8), 1-14. <https://doi.org/10.1038/nenergy.2017.108>
14. Luo X., Jiang S., Yan X., Chen C., Liu S., Zhan S., Zhang L. Aminoalkyldisiloxane compound as efficient high-temperature electrolyte additive for $\text{LiMn}_2\text{O}_4/\text{graphite}$ batteries. *Ionics* **2022**, *29* (1), 87-96. <https://doi.org/10.1007/s11581-022-04814-x>
15. Lavi O., Luski S., Shpigel N., Menachem C., Pomerantz Z., Elias Y., Aurbach D. Electrolyte solutions for rechargeable li-ion batteries based on fluorinated solvents. *ACS Appl. Energy Mater.* **2020**, *3* (8), 7485-7499. <https://doi.org/10.1021/acsaem.0c00898>
16. Kabra V., Birn B., Kamboj I., Augustyn V., Mukherjee P. P. Mesoscale machine learning analytics for electrode property estimation. *J. Phys. Chem. C* **2022**, *126* (34), 14413-14429. <https://doi.org/10.1021/acs.jpcc.2c04432>
17. Hu M., Pang X., Zhou Z. Recent progress in high-voltage lithium ion batteries. *J. Power Sources* **2013**, *237* 229-242. <https://doi.org/10.1016/j.jpowsour.2013.03.024>
18. Choi N. S., Chen Z., Freunberger S. A., Ji X., Sun Y. K., Amine K., Yushin G., Nazar L. F., Cho J., Bruce P. G. Challenges facing lithium batteries and electrical double-layer capacitors. *Angew. Chem. Int. Edit.* **2012**, *51* (40), 9994-10024. <https://doi.org/10.1002/anie.201201429>
19. Chen X., Zhang X. Q., Li H. R., Zhang Q. Cation-solvent, cation-anion, and solvent-solvent interactions with electrolyte solvation in lithium batteries. *Batteries & Supercaps* **2019**, *2* (2), 128-131. <https://doi.org/10.1002/batt.201800118>
20. Chen X., Yao N., Zeng B. S., Zhang Q. Ion-solvent chemistry in lithium battery electrolytes: From mono-solvent to multi-solvent complexes. *Fundamental Research* **2021**, *1* (4), 393-398. <https://doi.org/10.1016/j.fmre.2021.06.011>
21. Su C. C., He M., Amine R., Rojas T., Cheng L., Ngo A. T., Amine K. Solvating power series of electrolyte solvents for lithium batteries. *Energ. Environ. Sci.* **2019**, *12* (4), 1249-1254. <https://doi.org/10.1039/C9EE00141G>
22. Ding M. S., Xu K., Zhang S., Jow T. R. Liquid/solid phase diagrams of binary carbonates for lithium batteries part ii. *J. Electrochem. Soc.* **2001**, *148* (4), A299-A299. <https://doi.org/10.1149/1.1353568>
23. Klassen B., Aroca R., Nazri M., Nazri G. A. Raman spectra and transport properties of lithium perchlorate in ethylene carbonate based binary solvent systems for lithium batteries. *J. Phys. Chem. B* **1998**, *102* (24), 4795-4801. <https://doi.org/10.1021/jp973099d>
24. Wang Y., Balbuena P. B. Theoretical studies on cosolvation of li ion and solvent reductive decomposition in binary mixtures of aliphatic carbonates. *Int. J. Quantum Chem.* **2005**, *102* (5), 724-733. <https://doi.org/10.1002/qua.20466>
25. Uchida S., Kiyobayashi T. What differentiates the transport properties of lithium electrolyte in ethylene carbonate mixed with diethylcarbonate from those mixed with dimethylcarbonate? *J. Power Sources* **2021**, *511* 230423-230423. <https://doi.org/10.1016/j.jpowsour.2021.230423>
26. Kimura K., Hayashi K., Kiuchi H., Morita M., Haruyama J., Otani M., Sakaebe H., Fujisaki F., Mori K., Yonemura M., et al. Structural variation in carbonate electrolytes by the addition of li salts studied by x-ray total scattering. *Phys. Status Solidi B Basic Res.* **2020**, *257* (11), 2000100-2000100. <https://doi.org/10.1002/pssb.202000100>

27. Schechter A., Aurbach D., Cohen H. X-ray photoelectron spectroscopy study of surface films formed on Li electrodes freshly prepared in alkyl carbonate solutions. *Langmuir* **1999**, *15* (9), 3334-3342. <https://doi.org/10.1021/la981048h>
28. Zhang W., Wang Y., Lan X., Huo Y. Imidazolium-based ionic liquids as electrolyte additives for high-voltage Li-ion batteries. *Rev. Chem. Intermed.* **2020**, *46* (6), 3007-3023. <https://doi.org/10.1007/s11164-020-04128-5>
29. Kameda Y., Umebayashi Y., Takeuchi M., Wahab M. A., Fukuda S., Ishiguro S.-i., Sasaki M., Amo Y., Usuki T. Solvation structure of Li⁺ in concentrated LiPF₆-propylene carbonate solutions. *J. Phys. Chem. B* **2007**, *111* (22), 6104-6109. <https://doi.org/10.1021/jp072597b>
30. Berhaut C. L., Porion P., Timperman L., Schmidt G., Lemordant D., Anouti M. Litdi as electrolyte salt for Li-ion batteries: Transport properties in EC/DMC. *Electrochim. Acta* **2015**, *180* 778-787. <https://doi.org/10.1016/j.electacta.2015.08.165>
31. Wu X., Gong Y., Xu S., Yan Z., Zhang X., Yang S. Electrical conductivity of lithium chloride, lithium bromide, and lithium iodide electrolytes in methanol, water, and their binary mixtures. *J. Chem. Eng. Data* **2019**, *64* (10), 4319-4329. <https://doi.org/10.1021/acs.jced.9b00405>
32. Gottwald T., Sedlářiková M., Vondrák J. Conductivity of inorganic perchlorates dissolved in aprotic solvents. *ECS Trans.* **2017**, *81* (1), 47-55. <https://doi.org/10.1149/08101.0047ecst>
33. Berhaut Christopher L., Lemordant D., Porion P., Timperman L., Schmidt G., Anouti M. Ionic association analysis of Litdi, Lifsi and LiPF₆ in EC/DMC for better Li-ion battery performances. *RSC Adv.* **2019**, *9* (8), 4599-4608. <https://doi.org/10.1039/C8RA08430K>
34. Khomenko V., Raymundo-Piñero E., Béguin F. High-energy density graphite/ac capacitor in organic electrolyte. *J. Power Sources* **2008**, *177* (2), 643-651. <https://doi.org/10.1016/j.jpowsour.2007.11.101>
35. Marcus Y., Hefter G. Ion pairing. *Chem. Rev.* **2006**, *106* (11), 4585-4621. <https://doi.org/10.1021/cr040087x>
36. Han S. A salient effect of density on the dynamics of nonaqueous electrolytes. *Sci. Rep.* **2017**, *7* (1), 46718-46718. <https://doi.org/10.1038/srep46718>
37. Uchida S., Kiyobayashi T. How does the solvent composition influence the transport properties of electrolyte solutions? LiPF₆ and LiFSI in EC and DMC binary solvent. *Phys. Chem. Chem. Phys.* **2021**, *23* (18), 10875-10887. <https://doi.org/10.1039/D1CP00967B>
38. Abraham M. J., Murtola T., Schulz R., Páll S., Smith J. C., Hess B., Lindahl E. GROMACS: High performance molecular simulations through multi-level parallelism from laptops to supercomputers. *SoftwareX* **2015**, *1-2* 19-25. <https://doi.org/10.1016/j.softx.2015.06.001>
39. Bussi G., Donadio D., Parrinello M. Canonical sampling through velocity rescaling. *J. Chem. Phys.* **2007**, *126* (1), 014101. <https://doi.org/10.1063/1.2408420>
40. Berendsen H. J. C., Postma J. P. M., Van Gunsteren W. F., Dinola A., Haak J. R. Molecular dynamics with coupling to an external bath. *J. Chem. Phys.* **1984**, *81* (8), 3684-3690. <https://doi.org/10.1063/1.448118>
41. Essmann U., Perera L., Berkowitz M. L., Darden T., Lee H., Pedersen L. G. A smooth particle mesh ewald method. *J. Chem. Phys.* **1995**, *103* (19), 8577-8593. <https://doi.org/10.1063/1.470117>
42. Allen P., Tildesley D. J. *Computer simulation of liquids*. Clarendon Press: Oxford, **1987**.
43. Jorgensen W. L., Maxwell D. S., Tirado-Rives J. Development and testing of the OPLS all-atom force field on conformational energetics and properties of organic liquids. *J. Am. Chem. Soc.* **1996**, *118* (45), 11225-11236. <https://doi.org/10.1021/ja9621760>
44. Canongia Lopes J. N., Deschamps J., Pádua A. A. H. Modeling ionic liquids using a systematic all-atom force field. *J. Phys. Chem. B* **2004**, *108* (6), 2038-2047. <https://doi.org/10.1021/jp0362133>
45. Dodda L. S., Cabeza de Vaca I., Tirado-Rives J., Jorgensen W. L. Ligpargen web server: An automatic OPLS-AA parameter generator for organic ligands. *Nucleic Acids Res.* **2017**, *45* (W1), W331-W336. <https://doi.org/10.1093/nar/gkx312>
46. Damm W., Frontera A., Tirado-Rives J., Jorgensen W. L. OPLS all-atom force field for carbohydrates. *J. Comput. Chem.* **1997**, *18* (16), 1955-1970. [https://doi.org/10.1002/\(SICI\)1096-987X\(199712\)18:16<1955::AID-JCC1>3.0.CO;2-L](https://doi.org/10.1002/(SICI)1096-987X(199712)18:16<1955::AID-JCC1>3.0.CO;2-L)
47. Allen M. P., Tildesley D. J. *Computer simulation of liquids*. Oxford University Press: **2017**; Vol. 1. <https://doi.org/10.1093/oso/9780198803195.001.0001>

48. Frisch M. J., Trucks G. W., Schlegel H. B., Scuseria G. E., Robb M. A., Cheeseman J. R., Scalmani G., Barone V., Petersson G. A., Nakatsuji H., et al., Gaussian 16 rev. C.01. Gaussian, Inc., Wallingford CT: **2016**.
49. Mulliken R. S. Electronic population analysis on lcao-mo molecular wave functions. I. *J. Chem. Phys.* **1955**, 23 (10), 1833-1840. <https://doi.org/10.1063/1.1740588>
50. Breneman C. M., Wiberg K. B. Determining atom-centered monopoles from molecular electrostatic potentials. The need for high sampling density in formamide conformational analysis. *J. Comput. Chem.* **1990**, 11 (3), 361-373. <https://doi.org/10.1002/jcc.540110311>
51. Hayamizu K., Aihara Y., Arai S., Martinez C. G. Pulse-gradient spin-echo (1)h, (7)li, and (19)f nmr diffusion and ionic conductivity measurements of 14 organic electrolytes containing lin(so2cf3)2. *J. Phys. Chem. B* **1999**, 103 (3), 519-24. <https://doi.org/10.1021/jp9825664>
52. Wang J., Wang W., Kollman P. A., Case D. A. Automatic atom type and bond type perception in molecular mechanical calculations. *J. Mol. Graph. Model.* **2006**, 25 (2), 247-260. <https://doi.org/10.1016/j.jmgm.2005.12.005>
53. Wang J., Wolf R. M., Caldwell J. W., Kollman P. A., Case D. A. Development and testing of a general amber force field. *J. Comput. Chem.* **2004**, 25 (9), 1157-1174. <https://doi.org/10.1002/jcc.20035>
54. Borodin O., Smith G. D. Quantum chemistry and molecular dynamics simulation study of dimethyl carbonate: Ethylene carbonate electrolytes doped with lipf₆. *J. Phys. Chem. B* **2009**, 113 (6), 1763-1776. <https://doi.org/10.1021/jp809614h>
55. Kozlova S. A., Emelyanenko V. N., Georgieva M., Verevkin S. P., Chernyak Y., Schäffner B., Börner A. Vapour pressure and enthalpy of vaporization of aliphatic dialkyl carbonates. *J. Chem. Thermodyn.* **2008**, 40 (7), 1136-1140. <https://doi.org/10.1016/j.jct.2008.02.012>
56. Verevkin S. P., Toktonov A. V., Chernyak Y., Schäffner B., Börner A. Vapour pressure and enthalpy of vaporization of cyclic alkylene carbonates. *Fluid Phase Equilibr.* **2008**, 268 (1-2), 1-6. <https://doi.org/10.1016/j.fluid.2008.03.013>
57. Ganesh P., Jiang D.-e., Kent P. R. C. Accurate static and dynamic properties of liquid electrolytes for li-ion batteries from ab initio molecular dynamics. *J. Phys. Chem. B* **2011**, 115 (12), 3085-3090. <https://doi.org/10.1021/jp2003529>
58. Yu J., Balbuena P. B., Budzien J., Leung K. Hybrid dft functional-based static and molecular dynamics studies of excess electron in liquid ethylene carbonate. *J. Electrochem. Soc.* **2011**, 158 (4), A400-A400. <https://doi.org/10.1149/1.3545977>
59. Takeuchi M., Matubayasi N., Kameda Y., Minofar B., Ishiguro S.-i., Umebayashi Y. Free-energy and structural analysis of ion solvation and contact ion-pair formation of li⁺ with bf₄⁻ and pf₆⁻ in water and carbonate solvents. *J. Phys. Chem. B* **2012**, 116 (22), 6476-6487. <https://doi.org/10.1021/jp3011487>
60. Dudariev D., Logacheva K., Kolesnik Y., Kalugin O. Interparticle interactions and dynamics in bmimbf₄ and libf₄ solutions in propylene carbonate: Md simulation. *Kharkov Univ. Bull. Chem. Ser.* **2019**, (33), 54-64. <https://doi.org/10.26565/2220-637X-2019-33-04>
61. Humphrey W., Dalke A., Schulten K. Vmd: Visual molecular dynamics. *J. Mol. Graph.* **1996**, 14 (1), 33-38. [https://doi.org/10.1016/0263-7855\(96\)00018-5](https://doi.org/10.1016/0263-7855(96)00018-5)
62. Gans P., Gill J. B., Longdon P. J. Spectrochemistry of solutions. Part 21.—inner- and outer-sphere complexes of lithium with thiocyanate in acetonitrile solutions. *J. Chem. Soc., Faraday Trans. 1* **1989**, 85 (7), 1835-1839. <https://doi.org/10.1039/F19898501835>
63. Bachelin M., Gans P., Gill J. B. Spectrochemistry of solutions. Part 24.—li, na, k and bun₄n thiocyanates in methanol: Infrared spectroscopic evidence for ion pairing and hydrogen bonding. *J. Chem. Soc., Faraday Trans.* **1992**, 88 (22), 3327-3330. <https://doi.org/10.1039/FT9928803327>
64. Tenney C. M., Cygan R. T. Analysis of molecular clusters in simulations of lithium-ion battery electrolytes. *J. Phys. Chem. C* **2013**, 117 (47), 24673-24684. <https://doi.org/10.1021/jp4039122>
65. Bernardes C. E. S., Minas da Piedade M. E., Canongia Lopes J. N. The structure of aqueous solutions of a hydrophilic ionic liquid: The full concentration range of 1-ethyl-3-methylimidazolium ethylsulfate and water. *J. Phys. Chem. B* **2011**, 115 (9), 2067-2074. <https://doi.org/10.1021/jp1113202>
66. Hanke C. G., Lynden-Bell R. M. A simulation study of water-dialkylimidazolium ionic liquid mixtures. *J. Phys. Chem. B* **2003**, 107 (39), 10873-10878. <https://doi.org/10.1021/jp034221d>

67. Marekha B. A., Kalugin O. N., Idrissi A. Non-covalent interactions in ionic liquid ion pairs and ion pair dimers: A quantum chemical calculation analysis. *Phys. Chem. Chem. Phys.* **2015**, *17* (26), 16846-16857. <https://doi.org/10.1039/C5CP02197A>
68. Bernardes C. E. S. Aggregates: Finding structures in simulation results of solutions. *J. Comput. Chem.* **2017**, *38* (10), 753-765. <https://doi.org/10.1002/jcc.24735>
69. France-Lanord A., Grossman J. C. Correlations from ion pairing and the nernst-einstein equation. *Phys. Rev. Lett.* **2019**, *122* (13), 136001. <https://doi.org/10.1103/PhysRevLett.122.136001>
70. Hess B. Determining the shear viscosity of model liquids from molecular dynamics simulations. *J. Chem. Phys.* **2002**, *116* (1), 209-209. <https://doi.org/10.1063/1.1421362>

Received 16.04.2024

Accepted 07.06.2024

Д.С. Дударев^{*†}, Є.А. Голубенко^{*}, Р.М.Н. Джаллах[†], О.М. Калугін^{*}. Мікроструктура та транспортні властивості гексафторфосфату літію в бінарній суміші диметилкарбонату з етиленкарбонатом для молекулярно-динамічного моделювання

^{*}Харківський національний університет імені В.Н. Каразіна, хімічний факультет, майдан Свободи, 4, Харків, 61022, Україна

[†]Університет Тріполі, Педагогічний факультет Янзур, Тріполі, Лівія

Розчини солей Li⁺ в багатьох розчинниках що застосовуються в Li-іонних акумуляторах мають максимум кривій залежності електропровідності від концентрації електроліту. Для мікроскопічної інтерпретації цього явища для одного із найбільш популярних електролітів - розчинів LiPF₆ у бінарній суміші диметилкарбонату (DMC) / етиленкарбонату (EC) (1:1) - було проведено молекулярно-динамічне моделювання відповідних систем з вмістом солі 0.1, 0.5, 1.0, 1.5 and 2.0 M. Потенційні моделі для молекул DMC і EC були розроблені як комбінація двох різних силових полів: OPLS-AA і GAFF, щоб правильно відтворити коефіцієнти дифузії чистих розчинників. Структуру було проаналізовано з використанням функцій радіального розподілу (ФРР) та поточних координаційних чисел (ПКЧ). Результати показують, що катіон Li⁺ може утворювати контактні іонні пари (КІП) і сольваторозділені іонні пари (СРІП) у розчинах. Загальне координаційне число катіону залишається незмінним і становить близько 5.5-6.0 для всіх концентрацій. Крім того, молекули EC та аніони PF₆⁻ конкурують за позицію в першій координаційній оболонці катіона. Був проведений аналіз агрегатів за двома різними критеріями. Для них використовувалися дві різні відстані: мінімуми на ФРР і мінімум на другій похідній від ПКЧ. Також були отримані коефіцієнти дифузії для всіх компонентів розчинів і в'язкість модельованих систем. Коефіцієнти дифузії для всіх компонентів зменшуються, а значення в'язкості нелінійно зростають із збільшенням концентрації солі. Значення електропровідності були отримані зі значень коефіцієнтів дифузії іонів через співвідношення Нернста-Ейнштейна. Ці результати та різке збільшення в'язкості при 1.0 M і при більш високих концентраціях LiPF₆ узгоджуються з розрахованими експериментальними значеннями електропровідності.

Ключові слова: гексафторфосфат літію, диметилкарбонат, етиленкарбонат, локальна структура, транспортні властивості, іонна агрегація.

Надіслано до редакції 16.04.2024

Прийнято до друку 07.06.2024

Kharkiv University Bulletin. Chemical Series. Issue 42 (65), 2024